The Astrophysical Journal, 814:8 (12pp), 2015 November 20 doi:10.1088/0004-637X/814/1/8

AN OFF-NUCLEUS NONSTELLAR BLACK HOLE IN THE SEYFERT GALAXY NGC 5252

Minjin Kim[1,2], Luis C. Ho[3,4], Junfeng Wang[5], Giuseppina Fabbiano[6], Stefano Bianchi[7], Massimo Cappi[8], Mauro Dadina[8], Giuseppe Malaguti[8], and Chen Wang[5]
[1] Korea Astronomy and Space Science Institute, Daejeon 305-348, Korea
[2] University of Science and Technology, Daejeon 305-350, Korea
[3] Kavli Institute for Astronomy and Astrophysics, Peking University, Beijing 100871, China
[4] Department of Astronomy, School of Physics, Peking University, Beijing 100871, China
[5] Department of Astronomy and Institute of Theoretical Physics and Astrophysics, Xiamen University, Xiamen, Fujian 361005, China
[6] Harvard-Smithsonian Center for Astrophysics, 60 Garden Street, Cambridge, MA 02138, USA
[7] Dipartimento di Matematica e Fisica, Università degli Studi Roma Tre, via della Vasca Navale 84, I-00146 Roma, Italy
[8] INAF-IASF Bologna, I-40129 Bologna, Italy
Received 2015 July 27; accepted 2015 October 8; published 2015 November 10

ABSTRACT

We report the discovery of an ultraluminous X-ray source (ULX; CXO J133815.6+043255) in NGC 5252. This ULX is an off-nuclear point source, which is 22″ away from the center of NGC 5252, and has an X-ray luminosity of 1.5×10^{40} erg s^{-1}. It is one of the rare examples of a ULX, which exhibits clear counterparts in radio, optical, and UV bands. A follow-up optical spectrum of the ULX shows strong emission lines. The redshift of the [O III] emission line coincides with the systematic velocity of NGC 5252, suggesting that the ULX is gravitationally bound to NGC 5252. The flux of [O III] appears to be correlated with both X-ray and radio luminosity in the same manner as ordinary active galactic nuclei (AGNs), indicating that the [O III] emission is intrinsically associated with the ULX. Based on the multiwavelength data, we argue that the ULX is unlikely to be a background AGN. A more likely option is an accreting black hole with a mass of $\geqslant 10^4\ M_\odot$, which might be a stripped remnant of a merging dwarf galaxy.

Key words: black hole physics – galaxies: individual (NGC 5252) – X-rays: galaxies

1. INTRODUCTION

Ultraluminous X-ray sources (ULXs) are typically defined as bright and nonnuclear point sources with $L_{\text{X-ray}} > 10^{39}$ erg s^{-1}, substantially larger than the Eddington luminosity of stellar-mass black holes (BHs; but see King et al. 2001). They have been proposed as candidates of intermediate-mass ($10^2\ M_\odot < M_{\rm BH} < 10^5\ M_\odot$) BHs (IMBHs; Colbert & Mushotzky 1999). While IMBHs are a cosmologically important link between stellar-mass BHs and supermassive BHs (Volonteri 2010), they are very rare objects (e.g., Greene & Ho 2004). Thus, ULXs could have great implications for studying the IMBH population. However, ULXs are preferentially found in late-type or star-forming galaxies (e.g., Swartz et al. 2004). This might suggest that they originate from high-mass X-ray binaries (HMXBs; $20\ M_\odot < M_{\rm BH} < 100\ M_\odot$; e.g., Gao et al. 2003), which might belong to the high-mass end of stellar BHs rather than IMBHs. Such massive stellar BHs are known to form in low-metallicity environments (Mapelli et al. 2013b). In this scenario, the power of ULXs could be explained by either accretion at super-Eddington rates (e.g., Begelman 2002) or beamed emission (e.g., King et al. 2001). Thus, typical ULXs of moderate power ($L_{\rm X} < 2\text{–}5 \times 10^{40}$ erg s^{-1}) are occasionally regarded to be powered by HMXBs. However, ULXs exceeding this luminosity ($\geqslant 5\text{–}10 \times 10^{40}$ erg s^{-1}) are thought to imply supermassive BHs or IMBHs at their center (Swartz et al. 2011; but see Bachetti et al. 2014).

One of the most striking candidates for an IMBH is a hyperluminous X-ray source (HLX-1) in ESO 243−49 (S0 galaxy; Farrell et al. 2009). Its peak X-ray luminosity is $\sim 10^{42}$ erg s^{-1}, which makes HLX-1 the most luminous known ULX. It appears to have an optical counterpart. From the optical spectroscopy, Wiersema et al. (2010) found Hα emission, whose central wavelength is consistent with the redshift of the host galaxy. Since the X-ray luminosity is substantially larger than the Eddington luminosity of HMXBs, the BH mass is thought to be as large as $\sim 2 \times 10^4\ M_\odot$ (Godet et al. 2012). While the origin of HLX-1 is unclear, its photometric properties indicate that it might be a remnant of the nucleus of a merging companion galaxy (Mapelli et al. 2013a).

Here we present another ULX candidate IMBH, CXO J133815.6+043255. This ULX is found in the outskirts of NGC 5252. NGC 5252 is an early-type (S0) Seyfert 2 galaxy at a redshift of 0.0229. It is one of the best examples to present an extended biconical emission-line region up to ∼30 kpc from the nucleus (Tadhunter & Tsvetanov 1989). The ULX is located ∼10 kpc away from the center. In this paper, we investigate the origin of the ULX in NGC 5252 using multiwavelength data, including optical spectroscopic and UV/optical imaging data. The paper is organized as follows. In Section 2, we describe the observing method and procedures of data analysis. In Section 3, we present the observed properties of the ULX based on the multiwavelength data. In Section 4, we discuss the nature of the ULX. Throughout the paper we adopt $H_0 = 71$ km s^{-1} Mpc^{-1}, $\Omega_m = 0.27$, and $\Omega_\Lambda = 0.73$, yielding a luminosity distance to NGC 5252 of 98.4 Mpc.

2. DATA

2.1. Chandra X-Ray Observations

NGC 5252 was first observed with the *Chandra X-Ray Observatory* (Weisskopf et al. 2002) on 2003 August 11 for 60.1 ks (observation identification number [ObsID] 4054; PI: M. Dadina), using the spectroscopic array of the Advanced CCD Imaging Spectrometer (ACIS) detector (Garmire et al. 2003) in the 1/4 subarray mode. The nucleus of NGC

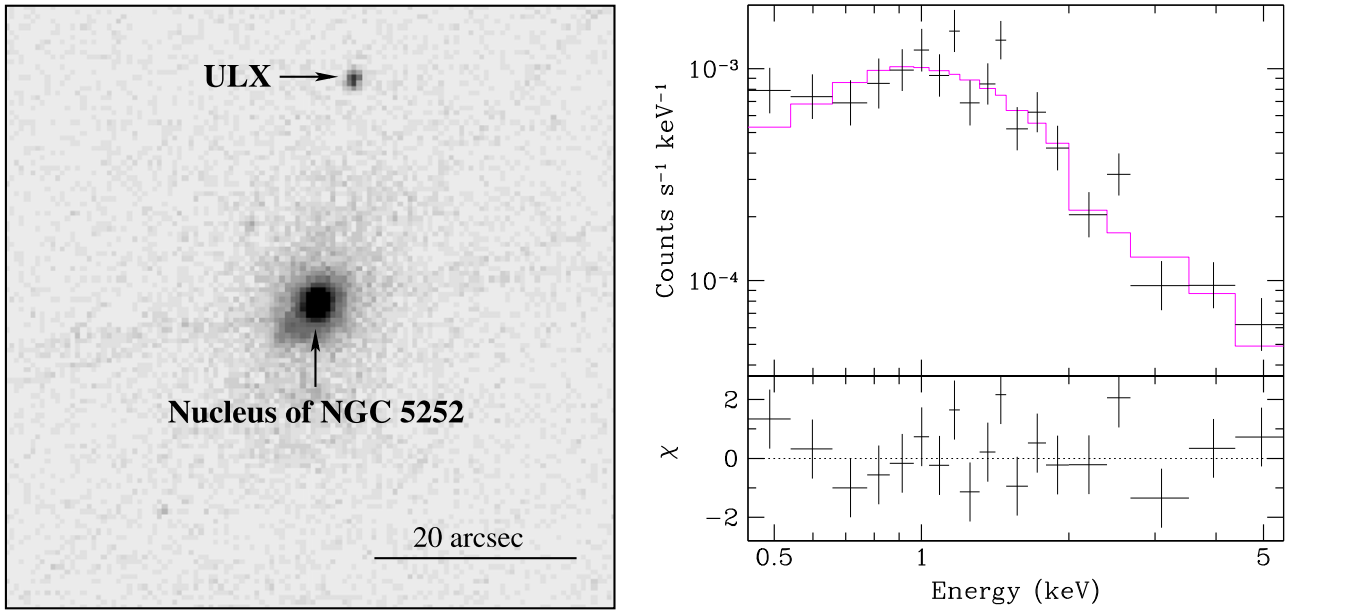

Figure 1. Left: *Chandra* ACIS-S image of NGC 5252 in the 0.3–8 keV band, centered on the X-ray-bright NGC 5252 active nucleus. The ULX is located to the north as indicated. North is up and east is left. Right: X-ray spectrum of the ULX and the best-fit absorbed power-law model (magenta line).

5252 was placed near the aimpoint on the backside-illuminated S3 chip, and the data telemetry mode was set to "Very Faint." Three more ACIS-S observations with the same configuration were obtained on 2013 March 4, March 7, and May 9, with exposure times of 40.4, 67.8, and 62.5 ks, respectively (ObsIDs 15618, 15022, 15621; PI: J. Wang). The data were analyzed following the standard procedures using CIAO (Version 4.6) with CALDB (Version 4.5.9) provided by the *Chandra* X-ray Center (CXC). We reprocessed the event files using CIAO script `chandra_repro` to apply the latest version of relevant calibration. The light curve from regions free of bright sources on the S3 chip was used to identify time intervals of high background, and no further filtering was required for this data set. The total exposure time is 230.8 ks.

Although the *Chandra* observations were intended to image the diffuse X-ray emission in NGC 5252, a bright off-nuclear X-ray point source caught our attention besides the known X-ray-bright Seyfert nucleus. Using CIAO tool `wavdetect`, we have identified the source at a position of R.A. = 13:38:15.64 and decl. = +04:32:55.4. (Figure 1). The uncertainty (1σ) on the source position is $0\farcs3$.

2.2. Spectroscopic Observations

We obtained an optical long-slit spectrum using the Inamori-Magellan Areal Camera & Spectrograph (IMACS) on the Baade 6.5 m telescope at Las Campanas Observatory on 2013 May 29 UT. The data were taken with a $1\farcs5$ slit in grism mode (300 lines mm^{-1}). It covers 3900–8000 Å with a spectral resolution ranging from 650 to 1200. The sky was mostly clear but occasionally covered by thin cirrus clouds. The seeing was between $0\farcs6$ and $1\farcs0$. The observation was done in relatively low airmass (<1.35). The total integration time was 2 hr, divided into four exposures to avoid the saturation of the sky emission lines. The slit was aligned to cover the center of the galaxy and the ULX simultaneously so that we can gauge the contribution from the central active galactic nucleus (AGN) along the radius (Figure 2). The slit ($\sim30'$) is long enough to cover the entire galaxy and the sky. The spatial pixel size is $0\farcs2$ on the sky. Following the target observation, we took the arc spectrum and the flat frames for the calibration. The flux calibration was done with two standard stars (CD 32 and LTT 4816).

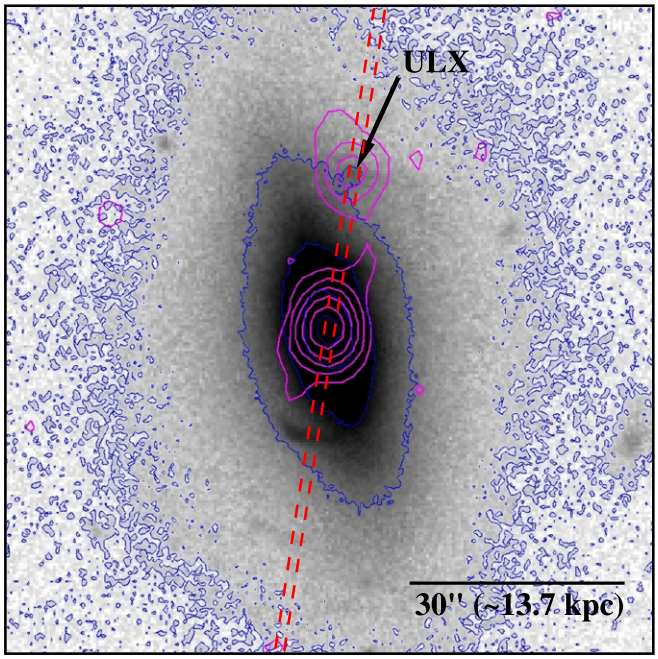

Figure 2. *g*-band image of NGC 5252 from the Sloan Digital Sky Survey. Blue contours represent the surface brightness. Magenta contours represent radio continuum at 20 cm from the FIRST survey. The ULX appears to have optical and radio counterparts. The long-slit position is denoted by the red dashed lines. North is up and east is left.

We reduced the data using IRAF. Flat-field correction was done using two sets of images (dome flats and sky flats). We used He+Ne+Ar arc lamp spectra for wavelength calibration. Spatial rectification was done using negative features made by

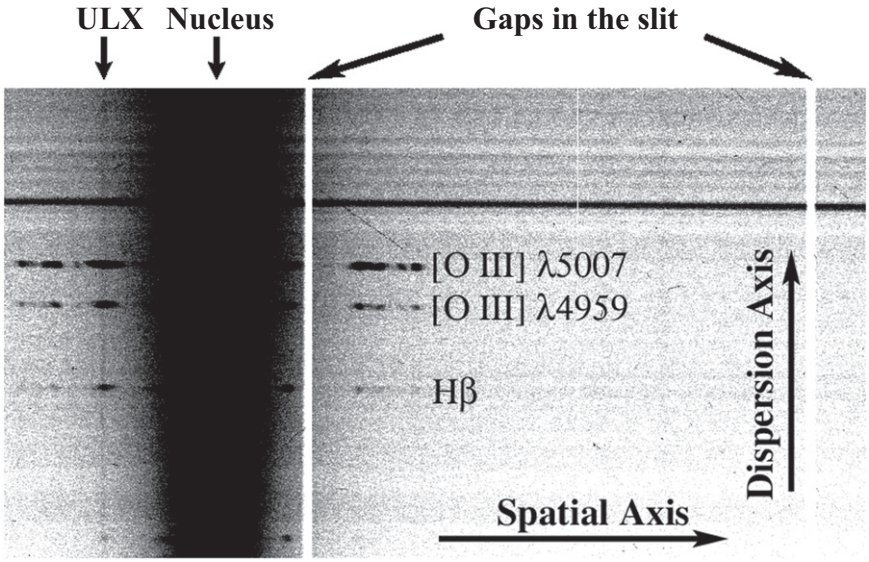

Figure 3. Part of two-dimensional spectrum of the nucleus of NGC 5252 and the ULX. The spatial extent is 170″. The positions of the ULX and the galaxy center are labeled. The continuum of the ULX is clearly seen. There are negative features along the dispersion axis, which are generated by the gaps in the slit mask. We use these features to calculate the distortion along the spatial axis.

blocked gaps in every ∼100″ along the long slit in the slit mask (see Figure 3). We combined the two-dimensional spectra using cosmic-ray rejection and applied the flux calibration. In order to see a spatial variance of the spectra, one-dimensional spectra with a width of 2″ were extracted. Finally, the spectra are corrected for Galactic extinction using the extinction curve of Fitzpatrick (1999).

At the position of the ULX, we extracted a spectrum with 2″ width and subtracted the local sky background in the vicinity of the source, so that we can remove the contribution from the galaxy. Throughout the paper, this spectrum is used for estimating the optical spectral properties of the ULX.

2.3. Photometric Observations

We assemble archival UV/optical imaging data taken with various telescopes (*Galaxy Evolution Explorer* (*GALEX*), *Hubble Space Telescope* (*HST*), Sloan Digital Sky Survey (SDSS), and Canada–France–Hawaii Telescope (CFHT)). Table 1 summarizes the archival data used in this paper. The data include 12 images obtained with far-UV (FUV), near-UV (NUV), F336W, *u*, FQUVN, *g*, F588N, F606W, *r*, F673N, *i*, and *z* filters. The basic data reduction steps of bias subtraction, flat-fielding, and alignment are carried out by the pipeline of each data set. For the data from *HST*, we use the `lacos_im` task (van Dokkum 2001) to remove cosmic rays. The flux calibration is also given by the pipeline, except the imaging data from the CFHT. We indirectly derive the zero point of the CFHT/*u* image by using the count rates of five bright stars with known magnitude from SDSS.

The ULX is visually detected in most images (Figure 4). But in FUV and *z*, it is unclear whether the counterpart is present at the position of the ULX. The position of the optical counterpart in the ground-based images is well matched with that derived in X-ray data within its positional uncertainty (0.″3). But the absolute astrometry of the *HST* images, especially those obtained before Cycle 14, which have a typical astrometric error of 1″–3″ due to the uncertainty of the guide star positions (Koekemoer et al. 2007), is not as accurate as other data. Thus, we correct the astrometry of the *HST* images using the sources with known positions from the SDSS images. However, owing to the narrow field of view and shallowness of the *HST* images, we were only able to use three faint sources for the registration. Given the typical astrometric error of the SDSS images (⩾0.″1; Pier et al. 2003), the uncertainties of the astrometry in the *HST* images might be slightly larger than 0.″1. We again find that the optical counterparts in the *HST* images are coincident with the X-ray position within 0.″5. Note that the aperture radii (0.″4–9″) for the aperture photometry are significantly larger than the astrometric uncertainties (∼0.″1) of the optical images, so that the photometric error due to the image misalignment should be negligible.

Table 1
Archival Imaging Data

Telescope/ Detector	Filter	Date	Exp. (s)	FWHM (″)	Aper. (″)
(1)	(2)	(3)	(4)	(5)	(6)
GALEX	FUV	2004 Apr 15	110	4.5	9.0
GALEX	NUV	2011 Apr 13	1620	5.0	9.0
HST/WFPC2	F336W	1994 May 09	3209	0.13	1.0
CFHT/MegaPrime	*u*	2009 Mar 30	530	1.56	2.4
HST/WFPC2	FQUVN	1994 May 09	3400	0.13	0.4
SDSS	*g*	2006 May 25	54	1.4	2.4
HST/WFPC2	F588N	1994 May 09	2400	0.13	1.0
HST/WFPC2	F606W	1994 Aug 23	500	0.13	1.0
SDSS	*r*	2006 May 25	54	1.3	2.4
HST/WFPC2	F673N	1994 May 09	1800	0.13	1.0
SDSS	*i*	2006 May 25	54	1.2	2.4
SDSS	*z*	2006 May 25	54	1.2	2.4

Note. Column (1): telescopes and detectors. Column (2): filters. Column (3): date of observation. Column (4): exposure time. Column (5): FWHM of the point-spread function (PSF). Column (6): radius for aperture photometry.

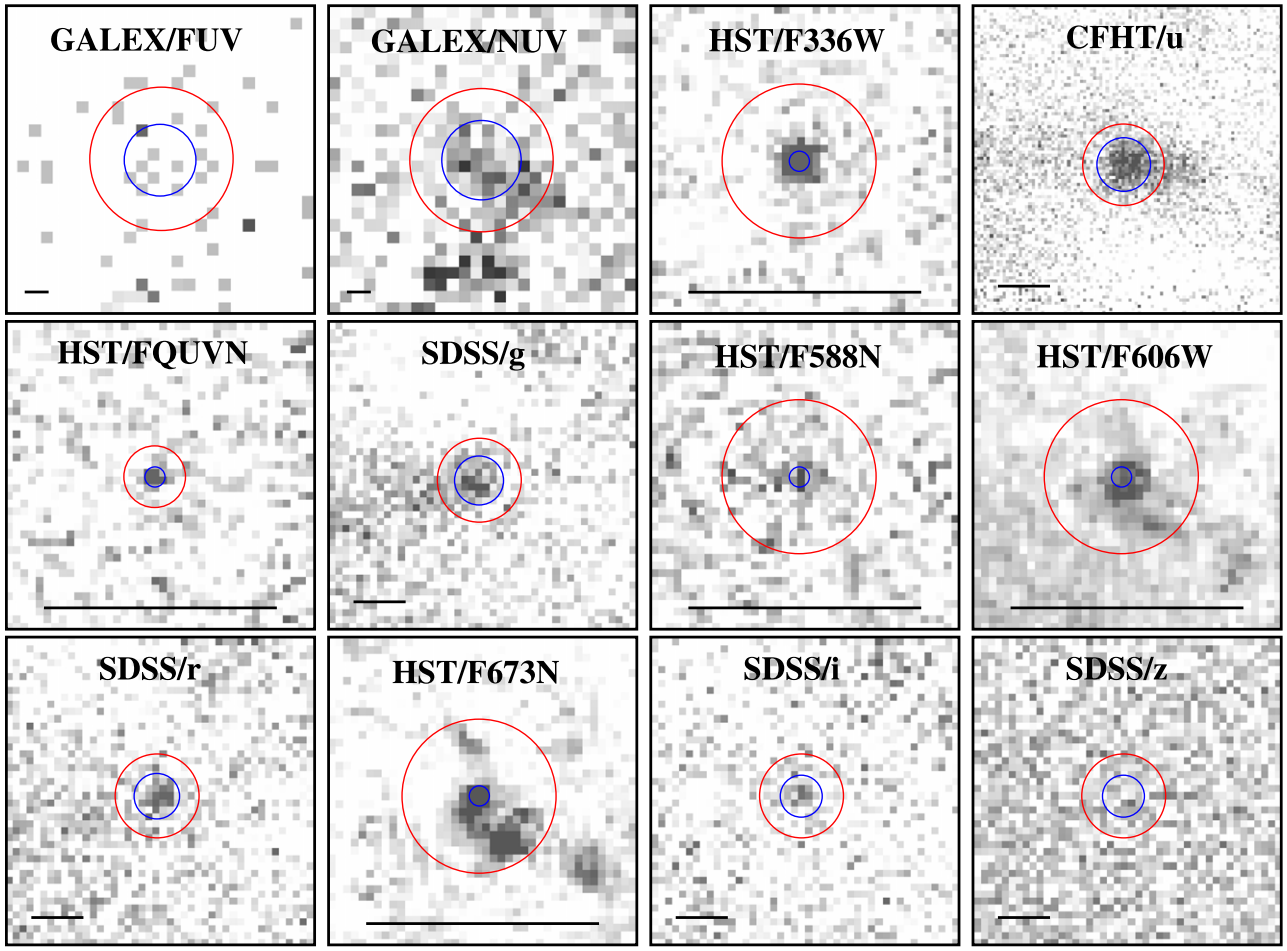

Figure 4. Postage-stamp images of the ULX from archival data (*GALEX*, *HST*, CFHT, SDSS), listed in order of increasing wavelength. Inner blue circles represent twice the size (FWHM) of the PSF. Outer red circles denote the radius for aperture photometry. The length of the bar at the bottom of each image corresponds to 3″. North is up and east is left for each image. All the sources are well matched with the position in the X-ray data within its astrometric uncertainty (∼0.″3). All images are presented in asinh stretch.

3. PROPERTIES OF THE ULX

3.1. X-Ray Properties

We extracted X-ray counts in the energy range of 0.3–8 keV from a circular region of 2.″5 radius centered at the source. Background was taken locally from an annular region also centered at the source. The total number of background-subtracted source counts is 391 ± 21. Spectra and instrument responses were generated and combined using `specextract`. Spectra were grouped to have a minimum of 20 counts per energy bin to allow for χ^2 fitting. The spectral modeling was performed with XSPEC version 12.7 (Arnaud 1996). We fit the X-ray spectrum with an absorbed power-law model. The fit prefers negligible intrinsic absorption, so we fixed the absorption column at the Galactic neutral hydrogen column density in the sightline toward NGC 5252, $N_{\rm H} = 1.97 \times 10^{20}\,{\rm cm}^{-2}$ (given by Dickey & Lockman 1990). The best-fit power-law photon index $\Gamma = 1.65 \pm 0.11$, with a reduced $\chi^2/{\rm dof} = 19.8/17$. Adding in an extra thermal emission or power-law component does not further improve the fit statistically. The absorption-corrected 0.5–8 keV flux is $(1.33 \pm 0.11) \times 10^{-14}\,{\rm erg\,cm^{-2}\,s^{1}}$. Adopting a distance of 98.4 Mpc to NGC 5252, this corresponds to $L_{\rm X} = 1.5 \times 10^{40}\,{\rm erg\,s^{-1}}$, placing the source into the ULX domain. We further examined the light curves for intra-observation and inter-observation variabilities and found no significant variations. Comparing to a constant light curve, the probability of variable signal is negligible in all cases. However, we found a long-term variability over 10 yr, evaluated using the count rates in 2003 and 2013. A χ^2 test against a constant light curve indicates that the probability for no variation is 0.0002, which implies that the long-term variation is statistically significant.

3.2. Spectral Properties

Strong narrow emission lines are found in the position of the ULX (Figure 5). The [O III] and Hα luminosities corrected for the extinction using the observed Balmer decrement (Hα/H$\beta \approx 3.9$) are as large as $10^{39.7}$ and $10^{39.2}\,{\rm erg\,s^{-1}}$, respectively. We note that these fluxes might be overestimated by 0.2 dex owing to the extended structures in the vicinity of the ULX (Section 3.3). Thus, if the lines are ionized by the source in the ULX, its energy is comparable to that of nearby low-luminosity AGNs (Ho 2008). However, it could also be ionized by the central AGN, which is ∼22″ away from the ULX.

Figure 6 shows distributions of [O III] flux and systematic velocity along the slit. As already known from previous studies, NGC 5252 harbors an extended narrow-line region (ENLR) up to a radius of 50″ (e.g., Tadhunter &

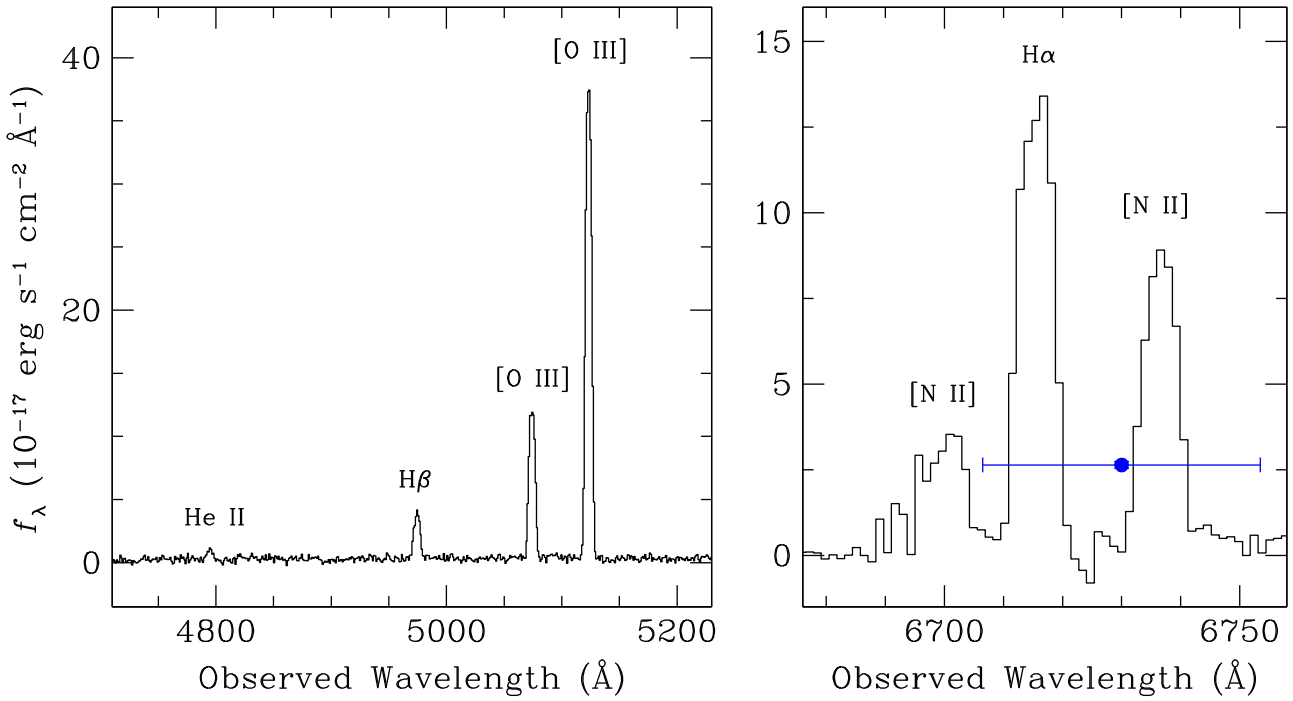

Figure 5. Optical spectrum at the position of the ULX extracted with an aperture width of 2″. In the right panel, we overplot the photometric measurement (blue circle) from the *HST* image obtained with the F673N filter.

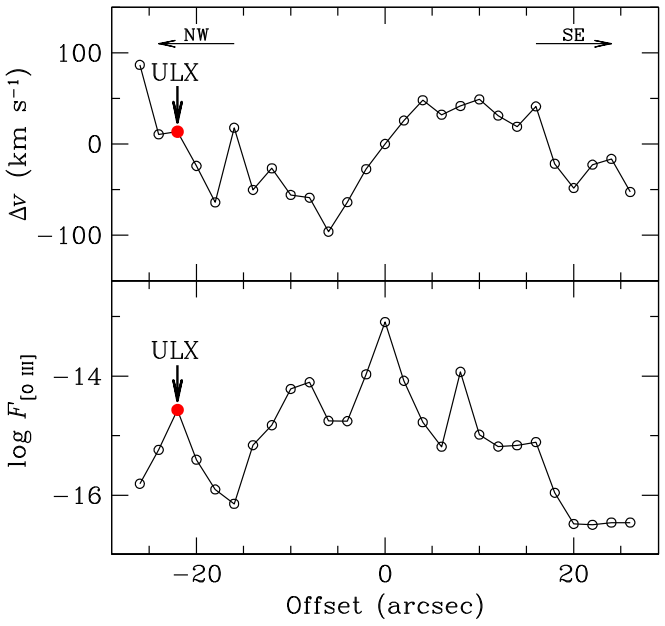

Figure 6. Distributions of [O III] λ5007 flux in units of erg s^{-1} cm^{-2} (bottom), and systematic velocity relative to the center (top), estimated from the peak of [O III] λ5007, as a function of radius. The ULX is located ∼22″ northwest of the center (red filled circle).

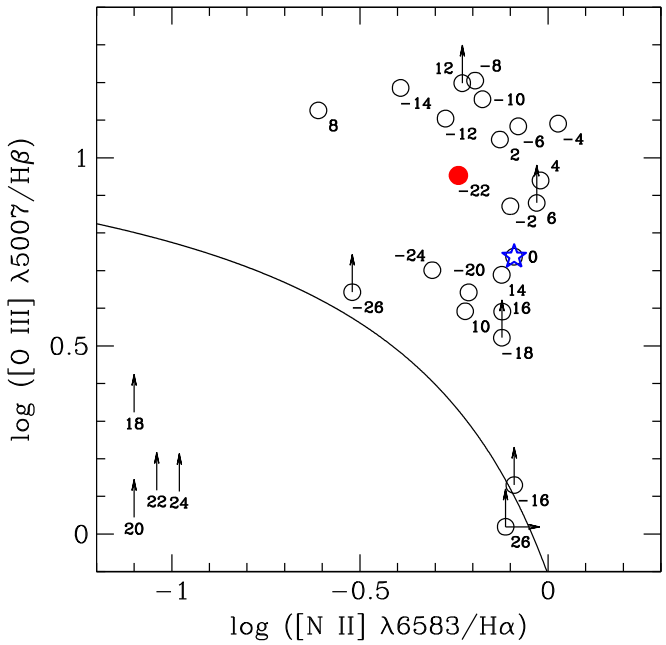

Figure 7. Distributions of optical line ratios for various positions. The distance from the center for each position in units of arcsec, which is the same as the offset in Figure 6, is denoted below the point. The center of NGC 5252 and the ULX are denoted by a blue star and a red filled circle, respectively. Data with no measurement of Hα and [N II] are plotted in the bottom left corner. The solid line shows the classification line between AGNs and star-forming galaxies, derived by Kewley et al. (2001).

Tsvetanov 1989). The ULX is located on the major axis of the ENLR. Acosta-Pulido et al. (1996) also reported an excess of line flux in [O III] and Hα close to the ULX, while the slit in their study is slightly off from the ULX (NW2 in Acosta-Pulido et al. 1996). Using the flux ratios among optical emission lines (Hβ, [O III] λ5007, Hα, [N II] λ6583), one can determine the source of ionizing radiation (Baldwin et al. 1981). Figure 7 indicates that the ENLR is mainly ionized by the AGN rather than hot stars from the star-forming region, which is in good agreement with previous studies (e.g., Acosta-Pulido et al. 1996). Since the strong X-ray emission, optical emission lines, and radio continuum can be associated with shocks (e.g., Sulentic et al. 2001; Konstantopoulos et al. 2014), it is worth testing this possibility. But the flux ratios among oxygen lines (log ([O III] λλ4363/5007) ≈ −1.9 and log ([O II] λ3727/[O III]

$\lambda5007) \approx -1.6$) lead us to rule out a significant contribution from the shocks (Dopita & Sutherland 1995; see also Morse et al. 1998).

Owing to the low instrumental spectral resolution ($\sigma_{\rm ins} \sim 100-200\,{\rm km\,s^{-1}}$), the emission lines are barely spectrally resolved at the position of the ULX. The velocity distribution shows a rotating pattern within $\sim5''$–$6''$ of radius from the nucleus, which is in good agreement with previous studies (Tsvetanov et al. 1996; Morse et al. 1998). But above that radius, the dynamics of the ionizing gas appears to be complicated. Interestingly, we note that the systematic velocity offset of the ULX relative to the nucleus of the galaxy is fairly small ($\sim13\,{\rm km\,s^{-1}}$). This indicates that the ULX might be gravitationally bound to NGC 5252.

Besides the strong emission lines, we find weak signs of underlying continuum (see Figure 3). The signal-to-noise ratio (S/N) of the continuum flux is $\approx$2.0 between $\sim$5000 Å and $\sim$8000 Å, while the S/N dramatically decreases ($\leqslant$1) below 4500 Å. Thus, the absolute flux calibration below 4500 Å may be very uncertain. Whereas the source of the continuum is unclear, the spectral energy distribution (SED) based on the broadband photometry suggests that it is not entirely explained by the stellar continuum unless the stellar population is very young ($\sim10^{6-7}$ yr). No broad component is detected in Hβ or Hα. We carefully examine the spectrum of the ULX to test the hypothesis that X-ray continuum comes from a background source. But we fail to find any signature (e.g., emission line, featureless continuum) of its existence. We will discuss this further in Section 4.2.

3.3. Photometric Properties

The high-resolution images from *HST* reveal that the optical counterpart is compact and marginally resolved (e.g., F336W), while there is a sign of extended features associated with the ULX in the low-resolution images (e.g., NUV, *u*, and *g*) and the *HST* images with narrowband filters affected by strong emission lines (e.g., F673N). Using the F336W image, which has the highest S/N among the images, we estimate the size of the optical counterpart. Using GALFIT (Peng et al. 2002; Peng et al. 2010), we fit the source by employing a synthetic PSF generated by TinyTim (Krist et al. 1995). We model the source with a Sérsic (Sérsic 1968) profile or a Gaussian profile. The best fit yields that the effective radius (r_e) is $\sim0\farcs1$ (46 pc). However, since the derived r_e is comparable to the size of the PSF, it thus shall be regarded as an upper limit. Even with this caveat, it is intriguing that this upper limit of the size is consistent with that of ultracompact dwarfs but significantly larger than that of globular clusters (e.g., Forbes et al. 2013).

Since the archival images are obtained with different detectors and in different observing conditions, it is important to measure the fluxes of the ULX in a consistent way. Moreover, it is crucial to remove the light of the host galaxy correctly because the gradient in the background can introduce an additional error on the photometric measurements. We model the host galaxy component with a Sérsic profile using GALFIT. We find that the host galaxy is well fit with two or three Sérsic components, but we do not ascribe physical significance to each individual component. After the host galaxy contribution is removed, we perform aperture photometry as a function of radius. The optimal aperture radius (red circles in Figure 4) is determined where the cumulative flux within the radius reaches a constant. If the source appears to be extended (e.g., *u* and F673N), we use the aperture radius determined from other images obtained with the same or a similar detector. Table 2 lists the flux measurements from the aperture photometry. While the flux in the FUV is very uncertain ($\sim$0.3 mag uncertainty), we note that it is also contained in the *GALEX* archival catalog (Morrissey et al. 2007); the catalog lists an AB magnitude of 20.58 mag, which is slightly brighter than, but within the uncertainty of, our measurement of 20.92 mag. Thus, our measurement in FUV is reliable.

Table 2
Photometric Measurements

Wavelength (1)	Magnitude (2)	Flux Density (3)	Flag (4)
1516	20.68 ± 0.27	$2.54 \pm 0.63 \times 10^{-16}$	−1
2267	21.43 ± 0.19	$5.67 \pm 0.99 \times 10^{-17}$	0
3344	21.66 ± 0.04	$2.11 \pm 0.08 \times 10^{-17}$	0
3499	21.65 ± 0.06	$1.95 \pm 0.11 \times 10^{-17}$	0
3900	21.97 ± 0.28	$1.17 \pm 0.30 \times 10^{-17}$	1
4728	21.49 ± 0.18	$1.23 \pm 0.20 \times 10^{-17}$	1
5894	22.60 ± 0.31	$2.86 \pm 0.80 \times 10^{-18}$	0
5997	22.34 ± 0.06	$3.50 \pm 0.21 \times 10^{-18}$	0
6200	21.87 ± 0.29	$5.06 \pm 1.37 \times 10^{-18}$	0
6732	19.90 ± 0.04	$2.64 \pm 0.10 \times 10^{-17}$	1
7615	21.69 ± 0.38	$3.95 \pm 1.37 \times 10^{-18}$	0
9054	20.95 ± 0.77	$5.56 \pm 3.92 \times 10^{-18}$	−1

Note. Column (1): central wavelength in units of Å. Column (2): magnitude in AB mag, corrected for Galactic extinction. Column (3): flux density (F_λ) corrected for Galactic extinction in units of erg s^{-1} cm^{-2} Å^{-1}. Column (4): flag: (−1) measurement is highly uncertain; (0) reliable measurement; (1) affected by strong emission line.

The F673N and F606W images show that there are faint, extended substructures to the southwest and northeast of the ULX, probably arising from Hα + [N II] emission. This emission likely lies partly or entirely within the aperture size of our extracted spectrum, although its nature and its association with the ULX are unclear. From aperture photometry of the F673N and F606W images with and without the substructures masked, we estimate that its contribution to the ULX spectrum is at most 40%. Therefore, it is possible that the luminosities of emission lines (e.g., [O III] and Hα) are overestimated by 0.2 dex owing to the substructures. Throughout this paper, we take this factor into account.

The optical counterpart is also detected by SDSS Data Release 7 (Abazajian et al. 2009). Their measurements are broadly in good agreement with ours in *g*, *r*, and *i*. But there is substantial discrepancy in *u* and *z*, which are much shallower than other bands. For the *u* band, we use a deeper image obtained with CFHT rather than that from SDSS. The flux from the *z* band is quite uncertain with an error of $\sim$0.77 mag.

We note that the flux density from the spectroscopy broadly agrees with the broadband photometry, except the blue part below 4000 Å (Figure 8). While it is unclear why the discrepancy is remarkable in the blue part, it indicates that there might be variability in the UV. This finding may be regarded as further evidence that the continuum source is nonstellar. Because we subtracted the local host galaxy light in the vicinity of the ULX when we extracted the spectrum (Section 2.2), the contribution from the host galaxy should be negligible.

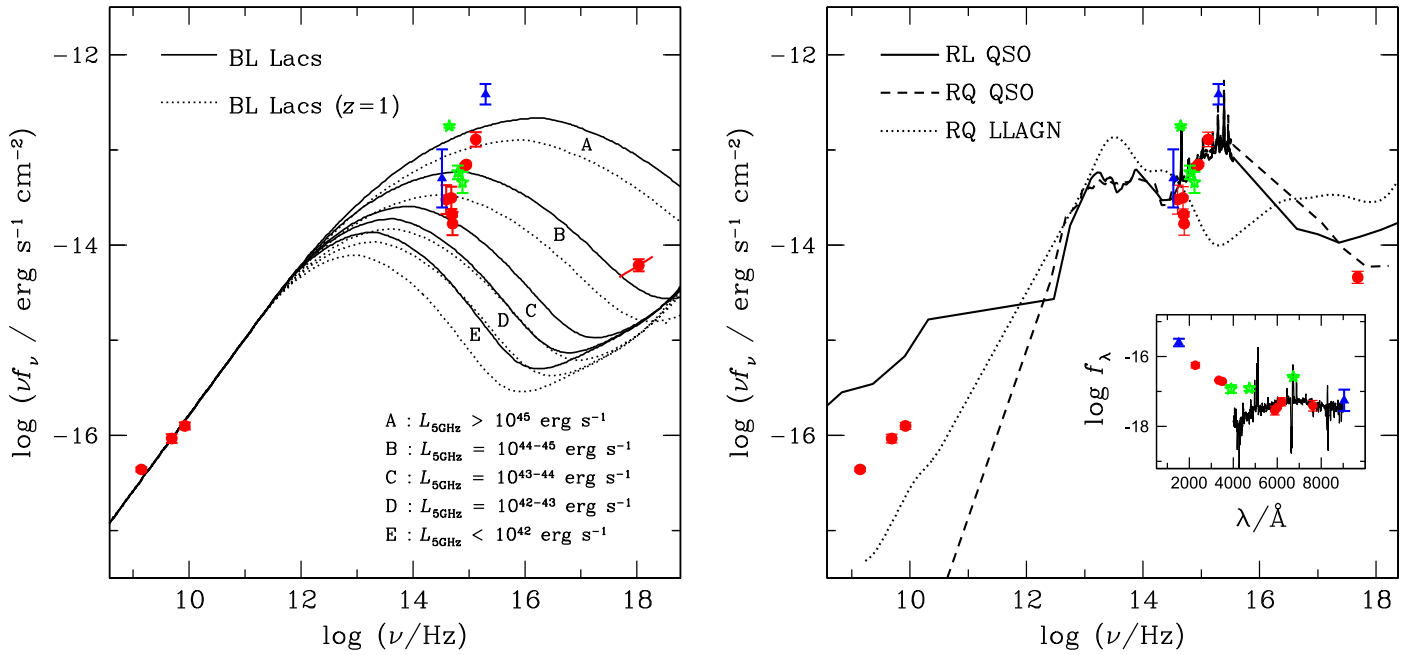

Figure 8. SED of the ULX, assuming that the ULX is located in NGC 5252. Ambiguous measurements are denoted by blue triangles. Photometric measurements affected by strong emission lines are denoted by green stars. Red circles represent robust measurements. Left: solid lines represent template SEDs of BL Lacs as a function of their radio luminosity (log $L_{5\ \mathrm{GHz}}$) from Donato et al. (2001; see also Fossati et al. 1998); dotted lines represent the same SEDs of BL Lacs but redshifted to $z = 1$. They are normalized to that of the ULX at 5 GHz. Right: solid and dashed lines denote SEDs of radio-loud (RL) and radio-quiet (RQ) quasars, respectively, from Shang et al. (2011). The dotted line shows the SED of radio-quiet low-luminosity AGNs ($L_{\mathrm{bol}}/L_{\mathrm{Edd}} < 10^{-3.0}$) from Ho (2008). SEDs of quasars and low-luminosity AGNs are normalized to that of the ULX at 6000 Å. In the inset, we overplot the optical spectrum of the ULX for comparison. The spectrum is smoothed using a Gaussian kernel for the purpose of display. Note that, for the purpose of display, the units of the inset are different from those of the larger panel.

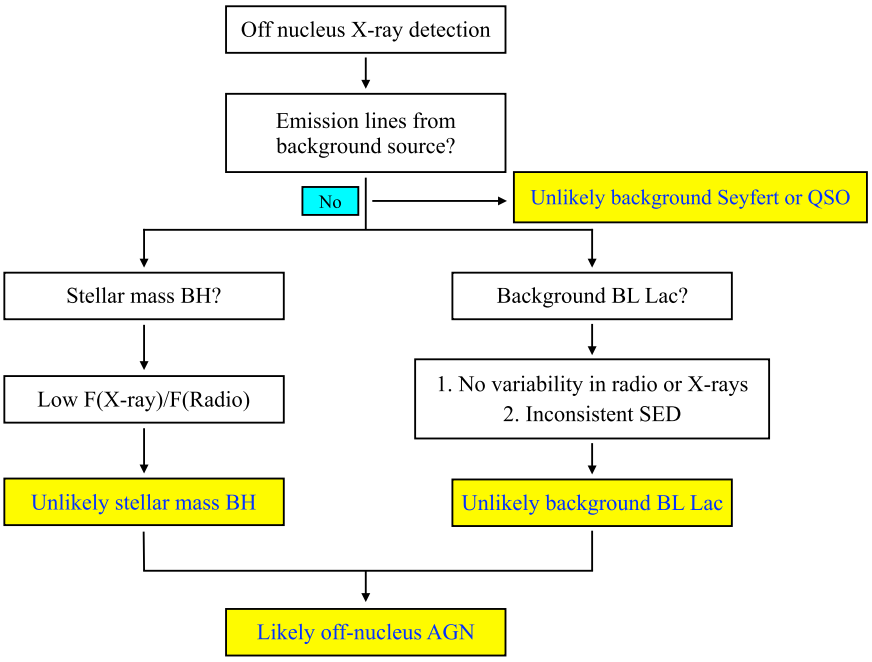

Figure 9. Flowchart for diagnosis of the nature of the ULX based on the observed photometric and spectroscopic properties.

3.4. Radio Data

Radio images of NGC 5252, obtained multiple times for ∼3 yr (from 1991 to 1993), show a source in coincidence with the position of the ULX (Wilson & Tsvetanov 1994; Becker et al. 1995; Kukula et al. 1995). The offset between the radio peak and the X-ray position of the ULX is smaller than 0.″3. The radio flux densities of the ULX are on average 1.50 ± 0.12 mJy, 1.9 ± 0.2 mJy, and 3.14 ± 0.06 mJy at 3.6, 6, and 20 cm, respectively. While the beam sizes of the radio images range from 0.″1 to 5″, the radio source at the position of the ULX is unresolved for all the radio data. The spectral index of the radio continuum between 3.6 and 20 cm of the counterpart of the ULX is ∼0.5 (α in $f_\nu \propto \nu^{-\alpha}$), which is consistent with that of nearby Seyferts (Ho & Ulvestad 2001). We find that the

variability over 3 yr is less than 10% at 3.6 and 20 cm (see also Wilson & Tsvetanov 1994).

4. NATURE OF THE ULX

We presented the spectroscopic and photometric properties of the optical counterpart of the ULX, obtained from the various telescopes and instruments. Based on this data set, we characterize and discuss its nature. The flowchart in Figure 9 briefly summarizes our approach to understanding the origin of the ULX.

4.1. The ULX Is Likely to Be Associated with NGC 5252

Strong emission lines are detected at the position of the ULX, and its velocity offset with respect to the center of NGC 5252 is remarkably small ($\sim$13 km s^{-1}). This suggests that the ULX is associated with NGC 5252. However, it is still inconclusive mainly because the emission lines underneath the ULX could be contamination from the ENLR. To address this issue, we investigate the profile of [O III] in the vicinity of the ULX. Intriguingly, we find a velocity gradient within a radius of 2″. As shown in Figure 10, the velocity inferred from the peak value of the [O III] line is maximized at radii of $\sim -2''$ and 1.″4 (916 and 640 pc), where the maximum velocities are -80 and 120 km s^{-1}, respectively. This strongly suggests that the line-emitting gas is affected by and therefore is physically associated with or in close proximity to the ULX. If so, then the ULX is not a background source but is physically located within NGC 5252.

While the [O III] line is barely resolved, it appears that the line dispersion slightly varies ($\Delta\sigma \leqslant 50$ km s^{-1}) within a radius of 2″, which indicates that the kinematics of the gas are affected by the ULX. This further suggests that the ULX is located within NGC 5252. The gas itself may be physically excited by the ULX, which appears to be powered by an active BH.

4.2. Unlikely to be a Background AGN

Although we do detect emission lines at the position of the ULX, it is still difficult to prove that the line emission comes from the ULX or is, instead, simply confused by the ENLR. Thus, it is worthwhile to consider whether the ULX might be an interloper. It is common that ULXs turned out to be foreground stars or background AGNs (Foschini et al. 2002; Masetti et al. 2003; Gutiérrez & López-Corredoira 2005; Wong et al. 2008; Gutiérrez 2013). Moreover, the incidence of background AGNs appears to be higher for ULXs found in early-type galaxies (e.g., Gutiérrez 2006; Heida et al. 2013).

As discussed in Section 3.2, we do not see any signs of emission lines, narrow or broad, from a background AGN in the spectrum. How strong should any hypothetical line emission be? We use the empirical correlation between X-ray and [O III] luminosity to estimate the strength of the expected optical line emission, if the source were a line-emitting background AGN. We adopt a conversion factor of $\log (L_{[\mathrm{O\,III}]}/10^{42}\ \mathrm{erg\ s^{-1}}) = 0.91\ \log(L_{2\,\mathrm{keV}}/10^{42}\ \mathrm{erg\ s^{-1}}) - 1.21$ based on type 1 AGNs (Stern & Laor 2012a, 2012b) to calculate the expected [O III] luminosity, given a rest-frame 2 keV luminosity estimated from the observed $\Gamma = 1.65$. [O III] can be detectable up to $z \sim 0.8$ owing to the wavelength limit of the spectrum. We expect an [O III] luminosity ranging from 10^{40} to 1.5×10^{42} erg s^{-1} at $0.1 < z < 0.8$. Given the S/N of the continuum of the optical spectrum, we can detect [O III], if it is unresolved at the instrumental resolution of our spectrum, up to $z \sim 0.8$ at a significance of 6σ. This estimate assumes negligible internal extinction, which is not unreasonable given the low observed X-ray column.

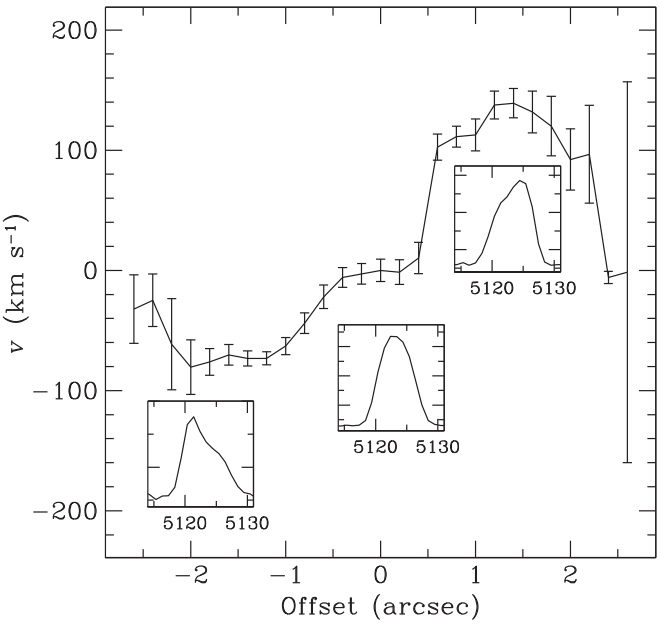

Figure 10. Velocity distribution derived from the peak of [O III] emission as a function of radius from the center of the ULX. From left to right inner panels, we plot profiles of [O III] at $-2''$ (NW), 0″, and 1.″4 (SE) away from the center, respectively.

Having ruled out the possibility that the ULX is a low-redshift AGN, we now evaluate whether it can be an AGN at $z > 0.8$. With $L_{2\mathrm{keV}} > 10^{43.5}$ erg s^{-1}, such a hypothetical source would be luminous enough to qualify as a type 2 quasar (e.g., Ptak et al. 2006), but the low observed column density is incompatible with the heavy obscuration typical of this class (Jia et al. 2013). At the same time, the featureless optical spectrum, which would correspond to rest-frame UV, is also inconsistent with that of a type 1 quasar. To estimate the expected strength of broad UV emission lines, we adopt the empirical scaling between the strength of the [O III] and Mg II and C IV, as well as the median line width of FWHM = 4500 km s^{-1}, as derived from the large SDSS quasar catalog of Shen et al. (2011). Given the S/N of our spectrum, we can rule out the existence of broad UV emission lines at the level of 10σ.

From the above analysis, we reject the possibility that the ULX is a line-emitting background AGN at any reasonable redshift. What about a weak-line AGN, namely, a BL Lac object? We argue against this possibility using three lines of evidence. The compactness of the radio source (Kukula et al. 1995) is consistent with the radio morphology of BL Lacs. First, the SED of the ULX does not look like that of typical BL Lacs (Fossati et al. 1998; Donato et al. 2001). The left panel of Figure 10 shows that there is substantial discrepancy, especially in the UV, between the SED of the ULX and those of BL Lacs. We varied the redshift but could not find any satisfactory solution that can simultaneously match the observed SED of the ULX in the UV and X-ray bands. One obvious weakness in this conclusion, of course, is that the SED

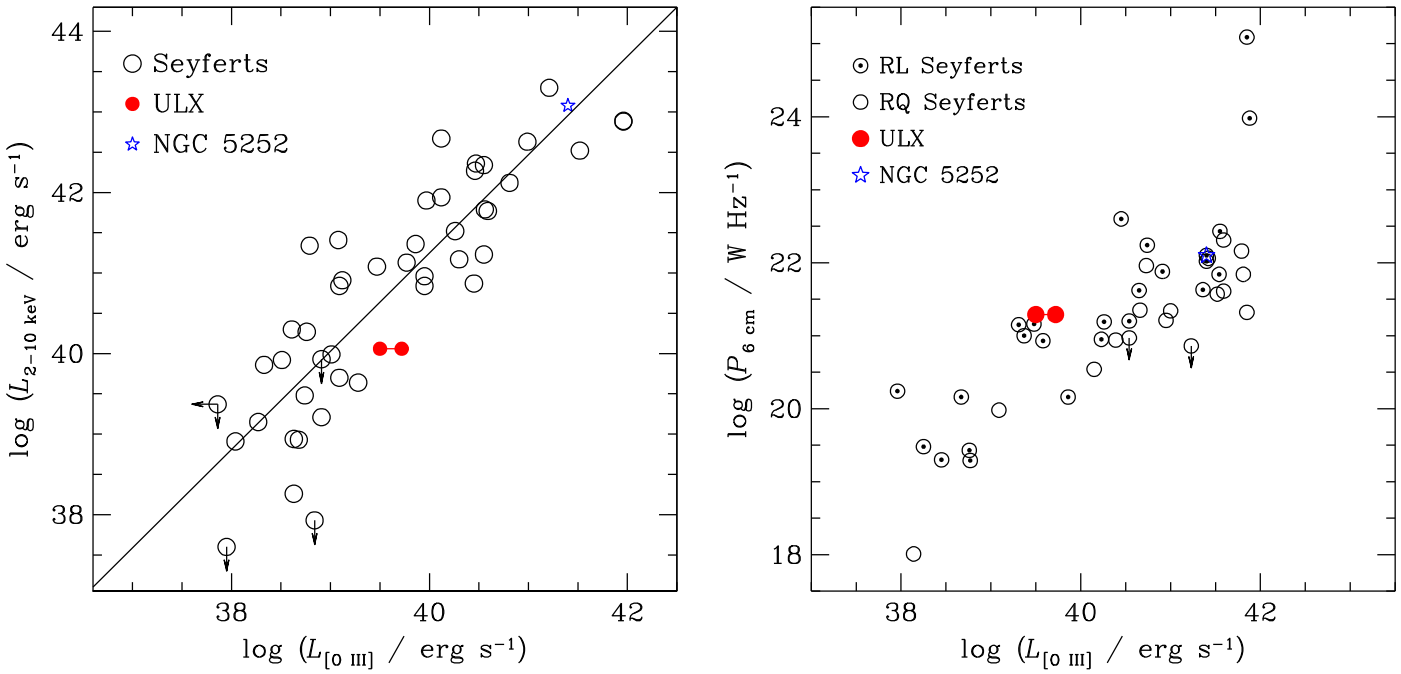

Figure 11. Left: correlation between [O III] and X-ray luminosity. Open circles and red filled circles show local Seyferts from Panessa et al. (2006) and the ULX from this study, respectively. The solid line represents the relation obtained from the local Seyferts. The nucleus of NGC 5252 is denoted by a blue star. The range of [O III] luminosities plotted for the ULX accounts for the uncertainty introduced by the effect of masking its nearby extended substructures (Figure 4). Right: correlation between [O III] and radio luminosity at 5 GHz. We plot radio-loud and radio-quiet Seyferts from Ho & Peng (2001). Typical uncertainties of the [O III] and radio luminosities are 0.3 dex and 5%, respectively.

measurements were not simultaneous, whereas BL Lac objects are known to be highly variable.

Second, the optical properties of the ULX do not agree with the expected properties of a BL Lac host. BL Lac objects are commonly hosted by massive (e.g., Falomo 1996; Urry et al. 1999; Kotilainen et al. 2005), luminous ellipticals with $M_R = -22.9 \pm 0.5$ mag (e.g., Sbarufatti et al. 2005). Thus, if the ULX is a BL Lac object, one can expect that the host galaxy would be detected in the *HST* images. By using the distribution of the apparent *R*-band magnitude of BL Lac host galaxies (Sbarufatti et al. 2005), we find that the host galaxy would have been detected if the ULX is a low-redshift BL Lac with $z < 0.4$. However, a high-z BL Lac cannot be ruled out as an interloper because the expected *r*-band host brightness for BL Lacs with $z \geqslant 0.4$ would be lower than our observational limits.

Finally, it is noteworthy that the ULX source does not vary in the radio by more than 10%. BL Lacs, by contrast, are highly variable (>10%) in the radio (Aller et al. 1992). However, it is possible that we do not have enough data to correctly judge the variability because the radio fluxes were obtained in only three different epochs within 3 yr. In order to test this possibility, we perform a Monte Carlo simulation by randomly choosing the data points at three different epochs from monitoring radio data of BL Lacs (Richards et al. 2011). We find that ∼40% of BL Lacs show variability less than 10%. This indicates that additional multiepoch data are needed to use radio variability to test whether the ULX is a background BL Lac. Interestingly, the X-ray data measured at three different epochs for 5 days also do not exhibit short-timescale variability at a level greater than 17%.

It is very intriguing that the SED of the ULX is roughly consistent with that of radio-loud quasars (Shang et al. 2011; see Figure 10, right panel). However, the lack of emission lines, as discussed above, is strongly at odds with this interpretation.

4.3. Not a Stellar-mass BH

As we discuss above, the probability that the ULX is a background AGN appears to be relatively low. Under the assumption that the X-rays, optical emission lines, and radio continuum are associated with the ULX, it is natural to suppose that it is an off-nucleus stellar-mass BH. For stellar-mass BH binaries, the X-ray flux is correlated closely with the radio flux (e.g., Corbel et al. 2003; Gallo et al. 2003). Using the empirical correlation from Gallo et al. (2003), we find that the expected radio flux density (∼0.003–0.022 mJy) is 2 orders of magnitude smaller than the observed flux value (∼1.5–3.1 mJy) if the ULX is a "low/hard"-state BH binary. For an X-ray binary to be as luminous in the radio as observed relative to the X-rays, it would have to be in the "very high" state (Fender et al. 2004). However, this is incompatible with the lack of X-ray and radio variability, which is typically observed in very high state X-ray binaries (Miyamoto et al. 1991; Kubota & Done 2004). In addition, the X-ray spectrum is expected to be very steep in the very high state ($\Gamma \geqslant 2.5$;Miyamoto et al. 1991; Hori et al. 2014), which is inconsistent with the value of $\Gamma = 1.65$ observed for the ULX. We thus argue that our source is unlikely to be a stellar-mass BH.

4.4. Off-nucleus Nonstellar BH

If the ULX is an off-nucleus nonstellar BH, for example, from the accretion of a tidally stripped galaxy nucleus, one can expect that the line emission should correlate with the ionizing continuum from the BH. To test this scenario, we use the well-known correlation between [O III] luminosity and X-ray

luminosity in AGNs (e.g., Bassani et al. 1999; Heckman et al. 2005). Figure 11 shows that the observed $L_X/L_{[O\,III]}$ of the ULX is comparable to that of local Seyferts. The X-ray luminosity from 2 to 10 keV is corrected for Galactic and intrinsic absorption. The [O III] luminosity is corrected for extinction using the observed Balmer decrement ($H\alpha/H\beta \approx 3.9$) and the extinction curve of Fitzpatrick (1999). As discussed in Section 3.3, the [O III] luminosity may have been overestimated by 0.2 dex. Thus, a lower limit of the [O III] luminosity is also displayed in Figure 11; however, this is not significant enough to change any of our conclusions. That the ULX follows the L_X–$L_{[O\,III]}$ relation of Seyferts suggests that the optical line emission is powered by the local X-ray continuum rather than the central AGN in the host galaxy. As expected, the nucleus of NGC 5252 also falls on the relation; the X-ray and [O III] luminosities are estimated within the nucleus region (Cruz-Gonzalez et al. 1994; Dadina et al. 2010). Since the X-ray and [O III] emissions are broadly extended, the luminosities might be slightly underestimated. But the amount of underestimation should be negligible because the flux contribution from the extended region is less than 1% (Dadina et al. 2010).

A correlation between radio power and line ([O III]) luminosity in bright AGNs has been reported by various studies (e.g., Rawlings et al. 1989; Miller et al. 1993). This relation appears to hold also for Seyferts (Ho & Peng 2001). We find that the observed luminosity ratio between [O III] ($\approx 10^{39.5-39.7}$ erg s^{-1}) and radio continuum at 5 GHz ($\approx 10^{21.3}$ W Hz^{-1}) is in broad agreement with Seyferts (Figure 11). Indeed, the ULX is bright enough in the radio to be classified as a radio-loud AGN. These findings suggest that the radio, X-ray continuum, and [O III] emission originate from the same source, namely, an off-nucleus nonstellar, presumably fairly massive BH.

If the ULX is an off-nucleus BH, what is its mass? In order to address this question, we investigate the physical properties of the ULX. In the hypothesis that the bolometric luminosity does not exceed the Eddington luminosity, we can estimate a lower limit of the BH mass from the observed luminosity (but see Abramowicz et al. 1988). The bolometric conversion factors for the [O III] and X-ray luminosity strongly depend on luminosity, in the sense that they ($L_{bol}/L_{[O\,III]}$ and $L_{bol}/L_{2-10\,keV}$) tend to be smaller for lower-luminosity AGNs (e.g., Ho 2008; Stern & Laor 2012b). Adopting the conversion equation from Stern & Laor (2012b), $L_{bol}/L_{[O\,III]} \sim 162$, which leads to $\mathbf{M}_{BH} > 10^{3.5}\,M_\odot$. We can carry out the same experiment using the X-ray luminosity. By adopting the bolometric conversion factor of 16–28 for low- and moderate-luminosity AGNs (Ho 2008), we estimate $M_{BH} \geqslant 10^{3.0-3.6}\,M_\odot$, consistent with the estimate based on [O III] luminosity.

The BH mass can also be independently estimated using the fundamental plane of BH accretion (Merloni et al. 2003), which is described as

$$\log L_R = 0.6 \log L_X + 0.78 \log M_{BH}, \quad (1)$$

where L_R is the luminosity at 5 GHz in units of erg s^{-1}, L_X is the luminosity at 2–10 keV in units of erg s^{-1}, and M_{BH} is the BH mass in units of $M_\odot$. By assuming that the ULX follows this relation, we find that M_{BH} is as large as $\sim 10^8\,M_\odot$ (Figure 12). While the fundamental plane has been recalibrated with various types of samples (e.g., Gültekin et al. 2009; Plotkin et al. 2012), our estimate does not change significantly if we adopt the revised versions. A caveat is that this empirical relation is only applicable for BHs accreting in the low state (i.e., $L_{bol}/L_{Edd} \leqslant 0.1$). If the BH mass is indeed as large as suggested by the fundamental plane relation, we are faced with a serious challenge. First, the Eddington ratio would be very low ($\sim 2 \times 10^{-5}$). Such a low Eddington ratio should produce a low-ionization parameter for the optical emission lines (Ho 2008, 2009), similar to those seen in low-ionization nuclear emission-line regions, which have [O III]/Hβ < 3 (Ho et al. 1997). Instead, the ULX is observed to have Seyfert-like line ratios, with [O III]/H$\beta \sim 9$.

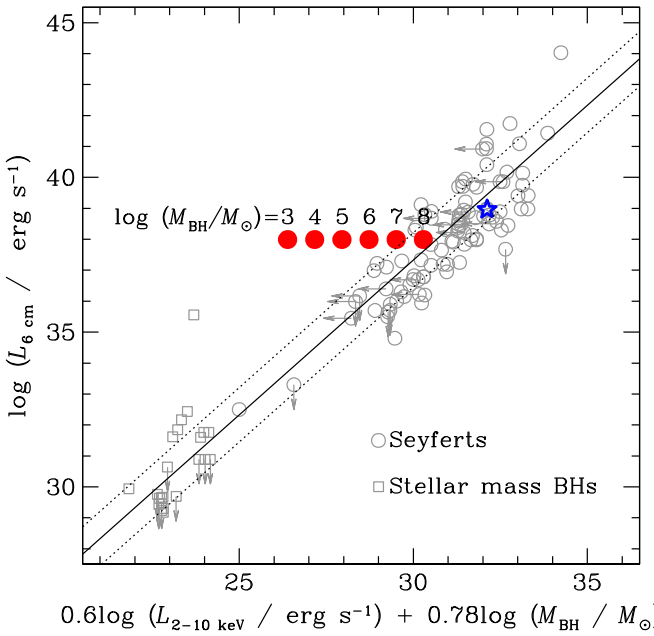

Figure 12. Fundamental correlation among radio luminosity, X-ray luminosity, and BH mass. Open gray circles and squares show the relation for local Seyferts and stellar-mass BHs, respectively (Merloni et al. 2003). The solid and dotted lines are the best fit and its 1σ scatter obtained by Merloni et al. (2003), respectively. The blue star represents the center of NGC 5252 ($M_{BH} = 1.3 \times 10^8 M_\odot$, inferred from a relation between BH mass and stellar velocity dispersion). Red filled circles show expected locations in the plane as a function of BH mass ($10^{3-8}\,M_\odot$) for the ULX.

If the ULX is really associated with a nonstellar mass BH, it raises the question about its nature. Morse et al. (1998) showed that the kinematics of the ionized gas in NGC 5252 can be modeled with at least three different components, which suggests an external origin of the gas. Although NGC 5252 is an early-type galaxy, it has abundant H I gas ($M_{HI} \sim 10^9 M_\odot$), and its structure is highly complicated (Prieto & Freudling 1996). Thus, it seems that NGC 5252 may have undergone a gas-rich merger. In this case, we might speculate that the off-nucleus BH powering the ULX is the remnant of an already-merged companion galaxy. If our estimation for the BH mass ($\sim 10^{4-8}\,M_\odot$) is correct, the merging galaxy should have had a bulge with stellar mass of $\sim 10^{7.0-10.4}\,M_\odot$, derived from the correlation between BH mass and bulge stellar mass (Kormendy & Ho 2013).

For comparison, we estimate the total stellar mass of NGC 5252 to be $M_* \approx 1.4 \times 10^{11}\,M_\odot$, using its K-band luminosity ($M_K = -24.55$ mag; Peng et al. 2006) and stellar velocity dispersion ($\sigma_* = 209$ km s^{-1}; Cid Fernandes et al. 2004)

following the conversions given in Kormendy & Ho (2013). If the ULX has a BH mass as large as $\sim 10^8\,M_\odot$, its progenitor bulge of $M_* \sim 10^{10.4}\,M_\odot$ implies that NGC 5252 experienced a fairly significant merger with a mass ratio of at least 1:6. This seems highly implausible, in view of the fact that NGC 5252 shows no evidence for any perturbation (tidal features, lopsidedness, etc.) in its current stellar distribution. On the other hand, it is not unreasonable that NGC 5252 could have accreted a small dwarf galaxy with $M_* \sim 10^7\,M_\odot$ that would have accompanied a $\sim 10^4\,M_\odot$ BH. Such a minor merger event should have little impact on the global structure of a galaxy 10^4 times more massive.

Unlike most ULXs studied to date, this particular ULX is unusual in that it has a prominent counterpart in the optical continuum. The physical nature of the optical continuum is unclear. We do not detect any obvious stellar features, but it is difficult to rule out that the continuum comes mainly from starlight, presumably the nucleus of a larger galaxy whose outer parts have already been stripped. In the following, we *assume* that the optical continuum is stellar and use it to place an upper limit on the stellar mass associated with the ULX. To minimize the possible contribution from the featureless continuum of the BH accretion disk, we use *i*-band photometry, which gives $M_i = -13.3$ mag. While mass-to-light ratio strongly depends on the initial mass function, metallicity, and age of the stellar population, we approximately estimate an upper limit of stellar mass of $\sim 10^8\,M_\odot$ using the stellar population synthesis models from Vazdekis et al. (2012) and Ricciardelli et al. (2012).

Interestingly, the properties of the ULX are comparable to those of an ultracompact dwarf galaxy (M60-UCD1) around NGC 4649 (Strader et al. 2013). M60-UCD1 is very compact ($r_e \approx 24$ pc) and one of the most luminous UCDs known ($M_g \approx -13.7$). There appears to be an X-ray source at the center of M60-UCD1, although its luminosity ($\sim 10^{38}$ erg s^{-1}) is significantly lower than that of the ULX studied here. While the origin of the X-ray emission is somewhat uncertain, it is very likely to originate from a massive BH at the center, rather than a stellar BH (Sivakoff et al. 2007; Strader et al. 2013; Seth et al. 2014). Strader et al. (2013) and Seth et al. (2014) argue that M60-UCD1 is a tidally stripped remnant of a merging galaxy, which is consistent with our expectation for the ULX in NGC 5252.

4.5. Comparison with HLX-1 and NGC 3341

Interestingly, the properties of the ULX in this study are somewhat similar to those of HLX-1 in ESO 243–39. Both of them seem to have BHs significantly larger than stellar-mass BHs, reside in early-type galaxies at similar distances ($z \sim 0.023$), and have optical counterparts. In addition, their origin is thought to be merging galaxies. However, at the same time, it is intriguing to note that there are significant differences between the two sources. The ULX in NGC 5252 shows much higher flux ratio of optical emission to X-ray continuum. The luminosity of Hα emission of the ULX in NGC 5252 is $\sim 40-90$ times greater than that of HLX-1 (Wiersema et al. 2010), whereas the X-ray luminosity of the ULX in NGC 5252 is only 1%–65% of that of HLX-1 (Servillat et al. 2011). This implies that the difference in $L_{\rm X}/L_{\rm H\alpha}$ between the two sources is a factor of 90–9000. Moreover, the radio flux density of the ULX in NGC 5252 is at least ~ 40 times larger than that of HLX-1 (Webb et al. 2012). This might suggest that they have distinctive physical properties (e.g., BH mass and/or accretion rate).

NGC 3341 is another interesting case of an off-nucleus source exhibiting AGN signatures in both the optical and X-rays (Barth et al. 2008; Bianchi et al. 2013). Optical images of NGC 3341 clearly show evidence of ongoing merging with multiple companions (Barth et al. 2008). The off-nucleus AGN appears to be associated with a dwarf galaxy, indicating that this AGN might be triggered during ongoing minor mergers.

5. SUMMARY

We report the serendipitous discovery of a ULX located 10 kpc from the type 2 Seyfert nucleus of NGC 5252, an S0 galaxy known to contain an extended narrow-line region. The ULX has an intrinsic 2–10 keV X-ray luminosity of $L_X = 1.2 \times 10^{40}$ erg s^{-1}, and the X-ray spectrum can be well fit with a simple power law with a photon index of $\Gamma = 1.65 \pm 0.11$ with negligible intrinsic absorption column. No X-ray variability is detected within the observation window of 5 days.

The ULX has counterparts in the radio, optical, and UV bands. Follow-up optical spectroscopy reveals strong narrow emission lines characteristic of photoionization by an accretion-powered source. The redshift of the emission lines coincides precisely with the systemic velocity of NGC 5252. We argue that the [O III] emission, which is well correlated with both the X-ray and radio luminosity in the same manner as other AGNs, is intrinsically associated with the ULX, and that the emission in all bands arises from an accreting BH with a mass of at least $10^4\,M_\odot$, located within NGC 5252. Using a variety of arguments based on the optical spectrum and the broadband SED, we dismiss the possibility that the ULX is associated with a background AGN. We also consider improbable that the ULX is an X-ray binary system.

With a BH mass of $\geqslant 10^4\,M_\odot$, the progenitor host of the ULX appears to have been a small dwarf galaxy 10^4 times less massive than NGC 5252, which has since been accreted and assimilated into the larger galaxy.

We are grateful to an anonymous referee for helpful comments. We thank John Mulchaey and Elina Nieppola for useful suggestions and discussion. L.C.H. acknowledges support by the Chinese Academy of Science through grant No. XDB09030102 (Emergence of Cosmological Structures) from the Strategic Priority Research Program and by the National Natural Science Foundation of China through grant No. 11473002. J.W. and G.F. acknowledge NASA grant GO3-14117. J.W. acknowledges support from NSFC grants 11443003 and 11473021.

REFERENCES

Abazajian, K. N., Adelman-McCarthy, J. K., Agüeros, M. A., et al. 2009, ApJS, 182, 543
Abramowicz, M. A., Czerny, B., Lasota, J. P., & Szuszkiewicz, E. 1988, ApJ, 332, 646
Acosta-Pulido, J. A., Vila-Vilaro, B., Perez-Fournon, I., Wilson, A. S., & Tsvetanov, Z. I. 1996, ApJ, 464, 177
Aller, M. F., Aller, H. D., & Hughes, P. A. 1992, ApJ, 399, 16
Arnaud, K. A. 1996, in ASP Conf. Ser. 101, Astronomical Data Analysis Software and Systems V, ed. G. H. Jacoby & J. Barnes (San Francisco, CA: ASP), 17
Bachetti, M., Harrison, F. A., Walton, D. J., et al. 2014, Natur, 514, 202
Baldwin, J. A., Phillips, M. M., & Terlevich, R. 1981, PASP, 93, 5
Barth, A. J., Bentz, M. C., Greene, J. E., & Ho, L. C. 2008, ApJL, 683, L119
Bassani, L., Dadina, M., Maiolino, R., et al. 1999, ApJS, 121, 473

Becker, R. H., White, R. L., & Helfand, D. J. 1995, ApJ, 450, 559
Begelman, M. C. 2002, ApJL, 568, L97
Bianchi, S., Piconcelli, E., Pérez-Torres, M. Á., et al. 2013, MNRAS, 435, 2335
Cid Fernandes, R., Gu, Q., Melnick, J., et al. 2004, MNRAS, 355, 273
Colbert, E. J. M., & Mushotzky, R. F. 1999, ApJ, 519, 89
Corbel, S., Nowak, M. A., Fender, R. P., Tzioumis, A. K., & Markoff, S. 2003, A&A, 400, 1007
Cruz-Gonzalez, I., Carrasco, L., Serrano, A., et al. 1994, ApJS, 94, 47
Dadina, M., Guainazzi, M., Cappi, M., et al. 2010, A&A, 516, A9
Dickey, J. M., & Lockman, F. J. 1990, ARA&A, 28, 215
Donato, D., Ghisellini, G., Tagliaferri, G., & Fossati, G. 2001, A&A, 375, 739
Dopita, M. A., & Sutherland, R. S. 1995, ApJ, 455, 468
Falomo, R. 1996, MNRAS, 283, 241
Farrell, S. A., Webb, N. A., Barret, D., Godet, O., & Rodrigues, J. M. 2009, Natur, 460, 73
Fender, R. P., Belloni, T. M., & Gallo, E. 2004, MNRAS, 355, 1105
Fitzpatrick, E. L. 1999, PASP, 111, 63
Forbes, D. A., Pota, V., Usher, C., et al. 2013, MNRAS, 435, L6
Foschini, L., Di Cocco, G., Ho, L. C., et al. 2002, A&A, 392, 817
Fossati, G., Maraschi, L., Celotti, A., Comastri, A., & Ghisellini, G. 1998, MNRAS, 299, 433
Gallo, E., Fender, R. P., & Pooley, G. G. 2003, MNRAS, 344, 60
Gao, Y., Wang, Q. D., Appleton, P. N., & Lucas, R. A. 2003, ApJL, 596, L171
Garmire, G. P., Bautz, M. W., Ford, P. G., Nousek, J. A., & Ricker, G. R., Jr. 2003, Proc. SPIE, 4851, 28
Godet, O., Plazolles, B., Kawaguchi, T., et al. 2012, ApJ, 752, 34
Greene, J. E., & Ho, L. C. 2004, ApJ, 610, 722
Gültekin, K., Cackett, E. M., Miller, J. M., et al. 2009, ApJ, 706, 404
Gutiérrez, C. M. 2006, ApJL, 640, L17
Gutiérrez, C. M. 2013, A&A, 549, A81
Gutiérrez, C. M., & López-Corredoira, M. 2005, ApJL, 622, L89
Heckman, T. M., Ptak, A., Hornschemeier, A., & Kauffmann, G. 2005, ApJ, 634, 161
Heida, M., Jonker, P. G., Torres, M. A. P., et al. 2013, MNRAS, 433, 681
Ho, L. C. 2008, ARA&A, 46, 475
Ho, L. C. 2009, ApJ, 699, 626
Ho, L. C., Filippenko, A. V., & Sargent, W. L. W. 1997, ApJ, 487, 568
Ho, L. C., & Peng, C. Y. 2001, ApJ, 555, 650
Ho, L. C., & Ulvestad, J. S. 2001, ApJS, 133, 77
Hori, T., Ueda, Y., Shidatsu, M., et al. 2014, ApJ, 790, 20
Jia, J., Ptak, A., Heckman, T., & Zakamska, N. L. 2013, ApJ, 777, 27
Kewley, L. J., Dopita, M. A., Sutherland, R. S., Heisler, C. A., & Trevena, J. 2001, ApJ, 556, 121
King, A. R., Davies, M. B., Ward, M. J., Fabbiano, G., & Elvis, M. 2001, ApJL, 552, L109
Koekemoer, A. M., Aussel, H., Calzetti, D., et al. 2007, ApJS, 172, 196
Konstantopoulos, I. S., Appleton, P. N., Guillard, P., et al. 2014, ApJ, 784, 1
Kormendy, J., & Ho, L. C. 2013, ARA&A, 51, 511
Kotilainen, J. K., Hyvönen, T., & Falomo, R. 2005, A&A, 440, 831
Krist, J. 1995, in ASP Conf. Ser. 77, Astronomical Data Analysis Software and Systems IV, ed. R. A. Shaw, H. E. Payne & J. J. E. Hayes (San Francisco, CA: ASP), 349
Kubota, A., & Done, C. 2004, MNRAS, 353, 980
Kukula, M. J., Pedlar, A., Baum, S. A., & O'Dea, C. P. 1995, MNRAS, 276, 1262
Mapelli, M., Annibali, F., Zampieri, L., & Soria, R. 2013a, MNRAS, 433, 849
Mapelli, M., Zampieri, L., Ripamonti, E., & Bressan, A. 2013b, MNRAS, 429, 2298
Masetti, N., Foschini, L., Ho, L. C., et al. 2003, A&A, 406, L27
Merloni, A., Heinz, S., & Di Matteo, T. 2003, MNRAS, 345, 1057
Miller, P., Rawlings, S., & Saunders, R. 1993, MNRAS, 263, 425
Miyamoto, S., Kimura, K., Kitamoto, S., Dotani, T., & Ebisawa, K. 1991, ApJ, 383, 784
Morrissey, P., Conrow, T., Barlow, T. A., et al. 2007, ApJS, 173, 682
Morse, J. A., Cecil, G., Wilson, A. S., & Tsvetanov, Z. I. 1998, ApJ, 505, 159
Panessa, F., Bassani, L., Cappi, M., et al. 2006, A&A, 455, 173
Peng, C. Y., Ho, L. C., Impey, C. D., & Rix, H.-W. 2002, AJ, 124, 266
Peng, C. Y., Ho, L. C., Impey, C. D., & Rix, H.-W. 2010, AJ, 139, 2097
Peng, Z., Gu, Q., Melnick, J., & Zhao, Y. 2006, A&A, 453, 863
Pier, J. R., Munn, J. A., Hindsley, R. B., et al. 2003, AJ, 125, 1559
Plotkin, R. M., Markoff, S., Kelly, B. C., Körding, E., & Anderson, S. F. 2012, MNRAS, 419, 267
Prieto, M. A., & Freudling, W. 1996, MNRAS, 279, 63
Ptak, A., Zakamska, N. L., Strauss, M. A., et al. 2006, ApJ, 637, 147
Rawlings, S., Saunders, R., Eales, S. A., & Mackay, C. D. 1989, MNRAS, 240, 701
Ricciardelli, E., Vazdekis, A., Cenarro, A. J., & Falcón-Barroso, J. 2012, MNRAS, 424, 172
Richards, J. L., Max-Moerbeck, W., Pavlidou, V., et al. 2011, ApJS, 194, 29
Sbarufatti, B., Treves, A., & Falomo, R. 2005, ApJ, 635, 173
Sérsic, J. L. 1968, Atlas de Galaxias Australes (Córdoba: Obs. Astron., Univ. Nac. Córdoba)
Servillat, M., Farrell, S. A., Lin, D., et al. 2011, ApJ, 743, 6
Seth, A. C., van den Bosch, R., Mieske, S., et al. 2014, Natur, 513, 398
Shang, Z., Brotherton, M. S., Wills, B. J., et al. 2011, ApJS, 196, 2
Shen, Y., Richards, G. T., Strauss, M. A., et al. 2011, ApJS, 194, 45
Sivakoff, G. R., Jordán, A., Sarazin, C. L., et al. 2007, ApJ, 660, 1246
Stern, J., & Laor, A. 2012a, MNRAS, 423, 600
Stern, J., & Laor, A. 2012b, MNRAS, 426, 2703
Strader, J., Seth, A. C., Forbes, D. A., et al. 2013, ApJL, 775, L6
Sulentic, J. W., Rosado, M., Dultzin-Hacyan, D., et al. 2001, AJ, 122, 2993
Swartz, D. A., Ghosh, K. K., Tennant, A. F., & Wu, K. 2004, ApJS, 154, 519
Swartz, D. A., Soria, R., Tennant, A. F., & Yukita, M. 2011, ApJ, 741, 49
Tadhunter, C., & Tsvetanov, Z. 1989, Natur, 341, 422
Tsvetanov, Z. I., Morse, J. A., Wilson, A. S., & Cecil, G. 1996, ApJ, 458, 172
Urry, C. M., Falomo, R., Scarpa, R., et al. 1999, ApJ, 512, 88
van Dokkum, P. G. 2001, PASP, 113, 1420
Vazdekis, A., Ricciardelli, E., Cenarro, A. J., et al. 2012, MNRAS, 424, 157
Volonteri, M. 2010, A&ARv, 18, 279
Webb, N., Cseh, D., Lenc, E., et al. 2012, Sci, 337, 554
Weisskopf, M. C., Brinkman, B., Canizares, C., et al. 2002, PASP, 114, 1
Wiersema, K., Farrell, S. A., Webb, N. A., et al. 2010, ApJL, 721, L102
Wilson, A. S., & Tsvetanov, Z. I. 1994, AJ, 107, 1227
Wong, D. S., Chornock, R., & Filippenko, A. V. 2008, PASP, 120, 266